Chemical Engineering and Processing 50 (2011) 483–485

Contents lists available at ScienceDirect

Chemical Engineering and Processing: Process Intensification

journal homepage: www.elsevier.com/locate/cep

Invagination process induced by 2D desiccation of colloidal solutions☆,☆☆

L. Pauchard, M. Mermet-Guyennet, F. Giorgiutti-Dauphiné*

UPMC Univ Paris 6, Univ Paris-Sud, CNRS, UMR 7608, Lab FAST, Bat 502, Campus Univ, F-91405, Orsay, France

ARTICLE INFO

Article history:
Received 17 January 2010
Received in revised form 15 July 2010
Accepted 26 July 2010
Available online 3 August 2010

Keywords:
Drying
Colloid
Skin
Buckling

ABSTRACT

The drying process of a suspension of hard colloidal particles is investigated in a circular thin cell which ensures a two-dimensional radial drying. During solvent removal the concentration of particles accumulates to the liquid–gas interface and reaches the close packing concentration: a rigid skin forms. During the evaporation of water, the length of this rigid envelope keeps on decreasing till it stops shrinking. Then a buckling process occurs that leads to an inversion of the curvature. At this time and after a steady decrease, the envelope periphery starts to increase while its inner volume keeps decreasing. This deformation continues as the depressed region extends and invaginates inside the film. An experimental procedure coupling imaging of the skin formation and drying kinetics measurements provides a complete description of the successive mechanisms: drying process, formation of the rigid skin and invagination process.

1. Introduction

Desiccation of a film of complex fluids is an intricate phenomenon as it couples evaporation process, hydrodynamics and mechanical instabilities [1,2]. In particular, an increase of the concentration of the non-volatile species (e.g. particles and polymers) modifies the rheological properties of the medium. Also a thin film, dried on a substrate, is often strongly affected by the process of skin formation. These phenomena are crucial for coating technology since they give rise to major defects such as wrinkles, thus conditioning the final film quality. Here we consider an experimental procedure coupling imaging of the skin formation and drying kinetics characterization. In this way, a drop is sandwiched between two parallel circular glass slides. The quasi-2D geometry allows the drop to dry through a radial evaporation flux. In the ideal case of ultra pure solvents the drop completely evaporates as gas diffusion proceeds from the edge of the drop towards the edge of the cell. However in the case of a solution, non-volatile species are advected to the drop edge. Consequently the drop's contact lines remain pinned during a more or less long time as the drop progressively shrinks due to solvent loss. During this process the solute concentration near the drop edge becomes high; further accumulation of solute leads to a porous skin formation. Here the case of a suspension of hard colloidal particles leading to the formation of a porous envelope is reported. Strong distortions of the envelope take place during the drying process. A buckling process continued by an invagination takes place. The influence of the drop size and the wetting properties on the substrate on the envelope deformation are investigated.

2. Method

The experiments are performed using aqueous suspensions of hard nanolatex particles ($2a = 25$ nm) made of copolymer of styrene and acrylic acid (provided by Rhodia Recherche), at high particle volume fraction, 30%. Measurements of the surface tension of the solution give $\gamma \sim 62 \pm 5$ m Nm^{-1}, using the Wilhelmy Plate method with a tensiometer Krüss; the viscosity of the solution, measured using a rheometer Contraves LS30, is $\eta \sim 8$ mPa s. A few microliters of the suspension is placed in a thin cell made from two circular and parallel glass slides, 25 mm diameter (see Fig. 1). The slides are either carefully cleaned and dried or lubricated with a thin film of silicon oil *V1000*, providing different wetting conditions. A solution droplet is deposited onto the bottom slide then squeezed with the upper slide [3]; the gap between the slides is kept constant, 100 ± 10 μm, in our experiments. The simple geometry with the combination of video imaging (global view of the droplet) and optical microscopy (local view using a DM2500 Leica microscope with objective 10× magnification and Leica digital camera) allows for accurate visualization of the evolution of a droplet during the drying process. Also, using a fluorescent illumination, fluorescent imaging is performed adding an optimized ratio of tracer nanolatex particles (micromer®-greenF from Micromod, 15 nm in diameter) to the solution. Drying experiments are conducted at room tem-

☆ Presented at the 8th European Coating Symposium, September 7–9, 2009, Karlsruhe.

☆☆ ESC shall not be responsible for statements or opinions contained in papers or printed in its publications.

* Corresponding author.
E-mail address: fred@fast.u-psud.fr (F. Giorgiutti-Dauphiné).

0255-2701/$ – see front matter © 2010 Elsevier B.V. All rights reserved.
doi:10.1016/j.cep.2010.07.013

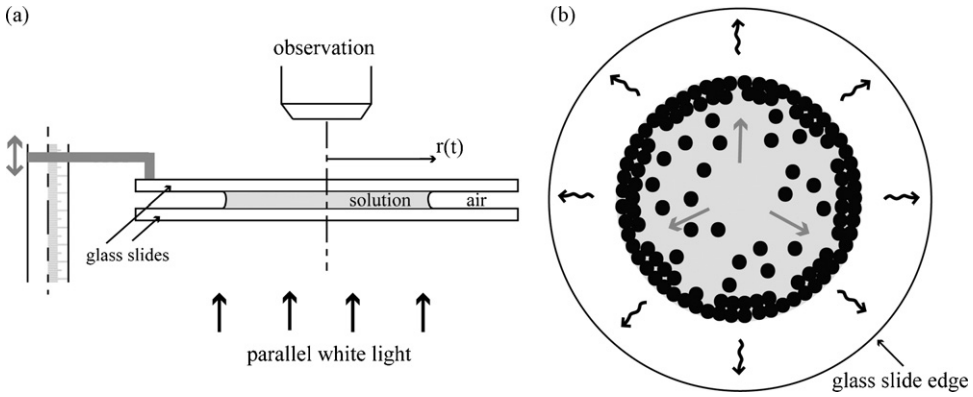

Fig. 1. (a) Set-up (side view): a droplet of solution (initial radius r_0) is sandwiched between two circular glass slides. The gap between both glass slides is controlled by a micrometer screw. The cell is illuminated by transmitted light. (b) Schematic illustration in top view showing the formation of a densely packed particles at the liquid–vapour interface during solvent removal.

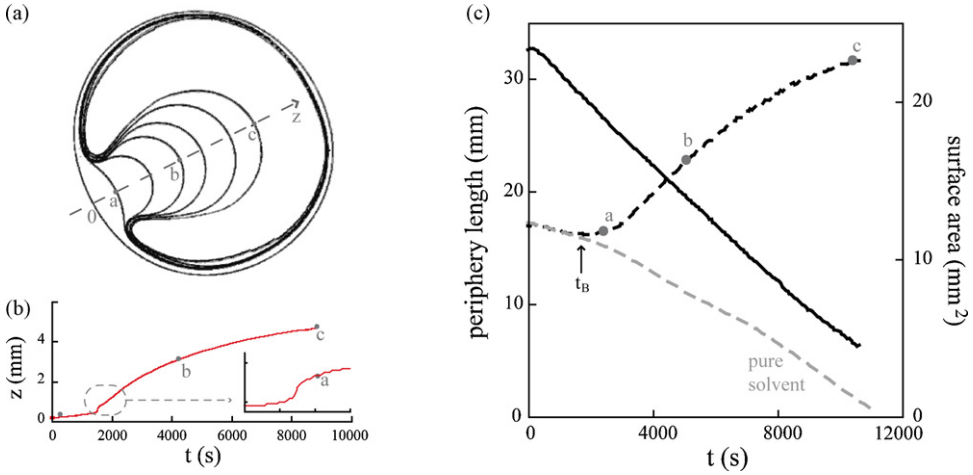

Fig. 2. (a) Superposition of digitized images taken at different times during the drying process of a droplet of colloidal suspension. (b) Time variations of the tip of the invagination along the z-axis. (c) Time variations in periphery length (dashed lines) and surface area (solid line); the grey dashed line corresponds to the case of a pure solvent droplet. Inversion of curvature takes place at t_B, says the buckling time.

perature and relative humidity $RH = 45 \pm 5\%$. Here, the transfer of water in air is limited by diffusion and therefore controlled by the relative humidity. During the drying process, the gas that escapes from the liquid–vapour interface is driven outward from the cell by diffusion. Consequently this empties the droplet and the particles are brought onto the liquid–vapour interface where their volume fraction grows (Fig. 1b) until the random close packing volume fraction.

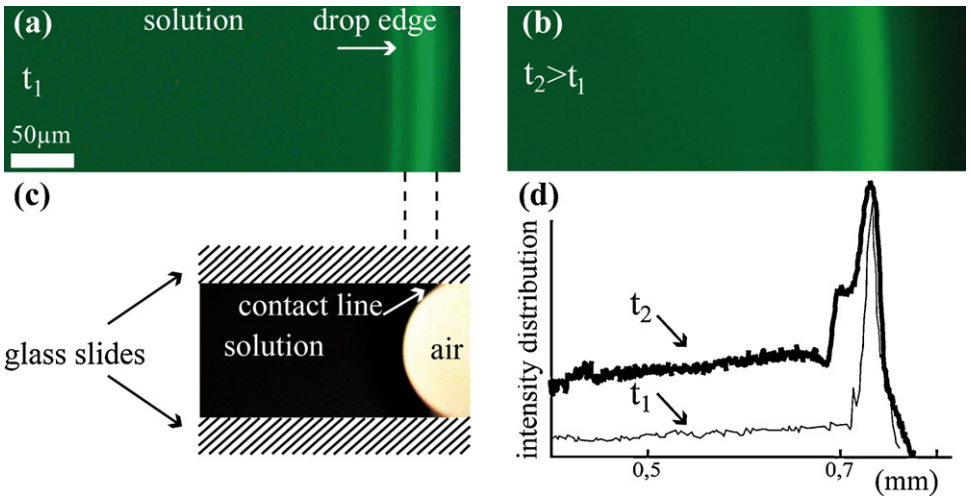

Fig. 3. (a and b) Fluorescence images, in top view, taken at two different times, denoted by t_1 and t_2, during the drying process. (c) Menisci at the droplet edge in side view (contact angle ~38°). (d) Intensity distribution corresponding to images (a) and (b) near the drop edge: the envelope thickness, h, increases during evaporation.

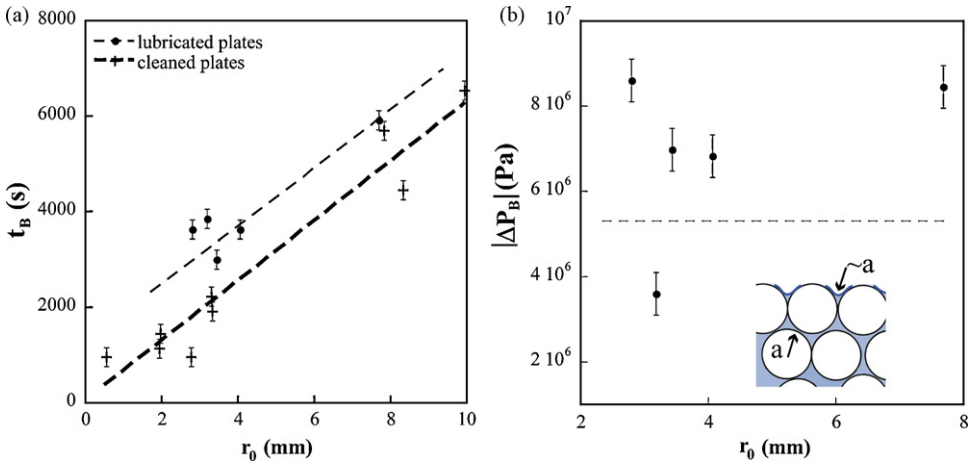

Fig. 4. (a) Buckling characteristic time, t_B, versus initial drop radius, r_0, in the case of glass slides lubricated (contact angle with the solution ~15°) or cleaned (contact angle ~38°). (b) Lubricated plates: calculated pressure drop, $|\Delta P_B|$, at buckling versus r_0. Dashed line corresponds to the estimated capillary pressure.

3. Results

Firstly the change in shape of the droplet is studied at a macroscopic scale. In a first stage, the drop progressively shrinks with solvent evaporation (Fig. 2a). As a result both periphery length and surface area decrease steadily with time (Fig. 2c). Then, contrasting with the case of a pure solvent, the droplet stops shrinking isotropically. In a second stage, a sudden inversion of curvature occurs (see dot *a* in Fig. 2a and b). This depression is continued by an invagination tip that deepens with time (Fig. 2a and b). As the surface area keeps decreasing, the periphery length starts increasing (Fig. 2c). At the final stage of the drying process, the distorted profile is pointed out by dot *c* in Fig. 2a. Experiments reveal that a single depression is always observed for different drying conditions ($RH < 10\%$ or >90%), whatever the droplet dimension, that is for droplets with radii in the range from 0.5 to 10 mm, chosen in comparison with the capillary length of the solution ~2.1 mm.

Secondly, we focus on a microscopic scale. At the beginning of the solvent loss, the outward flow convects the particles towards drop edge: a close-packed region forms, says the envelope formation (Fig. 1b). This so-called envelope thickens with time, which can be quantified by fluorescence microscopy images (Fig. 3a, b, and d).

With the chosen material, the envelope remains porous thus allowing further evaporation. Also, during solvent loss the envelope shrinkage is frustrated by another process: the pinning of the contact lines due to the deposition of particles there (Fig. 3c). By this way the porous envelope is submitted to large mechanical stresses. The competition between pinning/depinning process and shrinkage occurs and leads to a stick–slip motion of the contact line until this last remains strongly pinned at a location. Once a region of the envelope weakens, a buckling process occurs. Then the deformation is continued by invagination [4,5].

Let us note h_B and r_B are the envelope thickness and the drop radius at the buckling onset, respectively. Experiments reveal that the relative thickness, h_B/r_B, of the envelope at the point of buckling is independent of the initial size of the droplet, r_0 ($h_B/r_B \sim 0.058 \pm 0.012$ in our experimental conditions). Also the buckling time, t_B, linearly increases with r_0 (Fig. 4a). However, buckling process is altered by the contact line pinning. Therefore we investigate the case of droplets sandwiched between two lubricated glass slides, to minimize the pinning process. In these conditions, a single invagination still takes place but the buckling time is larger than in the case of cleaned glass slides (Fig. 4a). The limitation due to the pinning allows to treat the case of a purely elastic problem to describe the buckling process.

Also, let us consider the deformation to be driven by the pressure gradient governing the transport of a solvent of viscosity, η, through a porous medium of permeability, k, accordingly to Darcy law [1]. The permeability is the mean pore size, also pores connectivity, and can be estimated by the Carman–Kozeny relation: $k \sim 1\ \text{nm}^2$ for randomly packed monodisperse spheres. At the point of buckling the envelope is considered to be submitted to an external pressure such as:

$$\Delta P_B = P_i - P_c = -k^{-1} \eta V_E h_B \quad (1)$$

where P_i denotes the pressure inside the envelope and P_c the pressure at the external surface of the envelope; the evaporation rate, $V_E > 0$, is deduced from gravimetry measurements ($V_E \sim 10^{-7}$ m/s).

The pressure ΔP_B, calculated using expression (1) taking into account the experimental results, has the same order of magnitude than the capillary pressure ($\sim 2\gamma/a = 10^7$ Pa) due to air-solvent menisci between colloidal particles at the edge of the envelope as shown in inset in Fig. 4b [5]. Moreover, this value is in agreement with the critical elastic buckling load deduced from the linear buckling theory for shells, $\sim E \cdot (h_B/r_B)^2$ ($\sim 3.4 \times 10^6$ Pa), where E denotes the Young modulus of the porous envelope measured by micro-indentation testing ($E = 0.96 \pm 0.08$ GPa).

To conclude, we have presented preliminary results on drying experiments of a colloidal suspension in a simple geometry allowing direct imaging of a porous skin formation. During the drying process, the skin is submitted to high stresses. In particular providing certain wetting conditions on the substrates the pinning process of the three-phase line can be avoided. As a consequence the deformation of the envelope can be considered as the purely elastic problem of buckling instability. Broad perspectives emerge in the correlation between diffusion phenomenon driving skin formation and invagination induced by drying process.

Acknowledgement

We would like to thank E. Sultan for useful discussions and R. Pidoux for technical support.

References

[1] C.J. Brinker, G.W. Scherer, Sol–Gel Science, Academic Press, New York, 1990, pp. 453–488.
[2] J.L. Keddie, A.F. Routh, Latex Film Formation: With Applications in Nanomaterials, Springer Laboratory, 2009.
[3] F. Clément, J. Leng, Langmuir 20 (2004) 6538.
[4] L. Pauchard, Y. Couder, Europhys. Lett. 66 (5) (2004) 667.
[5] N. Tsapis, E.R. Dufresne, S.S. Sinha, C.S. Riera, J.W. Hutchinson, L. Mahadevan, D.A. Weitz, Phys. Rev. Lett. 94 (2005) 018302.